

Narrowband Vegetation Indices for Estimating Boreal Forest Leaf Area Index

Ellen Eigemeier, Janne Heiskanen, Miina Rautiainen, Matti Mõttus,
Veli-Heikki Vesanto, Titta Majasalmi and Pauline Stenberg
*University of Helsinki
Finland*

1. Introduction

1.1 Leaf area index

The green photosynthesizing leaf area of a canopy is an important characteristic of the status of the vegetation in terms of its health and production potential. At stand level, the amount of leaf area in a canopy is represented by a variable called the leaf area index (LAI), which is one of the key biophysical parameters in the global monitoring and mapping of vegetation by satellite remote sensing (Morisette et al., 2006). In this paper we adopt the, by now widely accepted, definition of LAI as the hemi-surface or half of the total surface area of all leaves or needles in the vegetation canopy divided by the horizontal ground area below the canopy. The definition is in line with the original definition of LAI, formulated for flat and (assumedly) infinitely thin leaves (Watson, 1947), as the one-sided leaf area per unit ground area. For coniferous canopies, the question arose on how to define the “one-sided” area of non-flat needles. While projected needle area formerly often has been used erroneously as a synonym to one-sided flat leaf area, it is now commonly accepted that the hemi-surface needle area represents the logical counterpart to the one-sided area of flat leaves (e.g. Chen & Black, 1992; Stenberg, 2006).

LAI controls many biological and physical processes, driving the exchange of matter and energy flow. Because LAI responds rapidly to different stress factors and changes in climatic conditions, monitoring of LAI yields a dynamic indicator of forest status and health. The link between forest productivity and LAI, in turn, lies in that LAI is the main determinant of the fraction of incoming photosynthetically active radiation absorbed by the canopy (fAPAR). The absorbed photosynthetically active radiation (APAR) quantifies the energy available for net primary production (NPP) and is thus a critical variable in NPP and carbon flux models. NPP is related to APAR by the light-use-efficiency originally introduced by Monteith (1977) for agricultural crops.

Traditionally, ground-based measurements of LAI have typically involved destructive sampling and determination of allometric relationships, e.g. between leaf area and the basal area of stem and/or branches carrying the leaves (the pipe model theory) (Shinozaki et al., 1964; Waring et al., 1982). However, such “direct methods” are quite laborious and indirect measurements of LAI using optical instruments are today the preferred choice (Welles &

Cohen, 1996; Jonckheere et al., 2004). They provide inverse estimates of LAI based on the fraction of gaps through the canopy in different directions, which can be measured using devices such as the LAI-2000 Plant Canopy Analyzer (LI-COR, 1992) or hemispherical photography. A vast body of classical literature exists on the dependency between LAI and canopy gap fraction underlying these techniques (e.g. Wilson, 1965; Miller, 1967; Nilson, 1971; Lang, 1986). In short, the inversion methods rely upon the assumption that leaves are randomly distributed in the canopy, in which case Beer's law can be applied to plant canopies (Monsi & Saeki, 1953). However, as the organization of leaves (needles) in forest canopies is typically more aggregated ("clumped") than predicted by a purely random distribution, the technique causes underestimation of LAI, especially in coniferous stands (e.g. Smith et al., 1993; Stenberg et al., 1994). Instead of the true LAI, the inversion of gap fraction data without correction for clumping yields the quantity commonly referred to as the "effective leaf area index" (Black et al., 1991).

Monitoring LAI in a spatially continuous mode and on a regular basis is possible only using remote sensing. Estimation of LAI from optical satellite images is considered feasible because LAI is closely linked to the spectral reflectance of plant canopies in the shortwave solar radiation range (Myneni et al., 1997). The physical relationships between canopy spectral reflectances and LAI form the basis of retrieval algorithms used in current Earth observation programs (e.g. MODIS, CYCLOPES, GLOBCARBON products) for mapping LAI at global scales. They produce bi-weekly and monthly vegetation maps that are widely used by biologists, natural resources managers, and climate modelers, e.g. to track seasonal fluctuations in vegetation or changes in land use. The arrival of narrowband reflectance data (also known as hyperspectral or imaging spectroscopy data) opens up new possibilities for satellite-derived estimation/monitoring of variables connected to the status and structure of vegetation, including LAI.

1.2 Spectral properties of boreal forests

The boreal forest zone, which spreads through Fennoscandia, Russia, Canada and Alaska, is the largest unbroken forest zone in the world and accounts for approximately one fourth of the world's forests. The boreal zone is a major store of carbon and thus plays an important role in determining global albedo and climate.

The reflectance spectra of coniferous forests (even if they have the same leaf area) are very distinct from similar broadleaved forests. The reasons for the special spectral behaviour of coniferous forests are versatile, yet primarily related to their structural, not optical, properties. Firstly, a high level of within-shoot scattering of conifers was originally noted nearly four decades ago (Norman & Jarvis, 1975). More recently, Landsat ETM+ data and a forest reflectance model were used to show that the low near infrared (NIR) reflectances observed in coniferous areas can largely be explained simply by within-shoot scattering (Rautiainen & Stenberg, 2005). Secondly, absorption by coniferous needles is higher than that by broadleaved species (Roberts et al., 2004; Williams, 1991), a phenomenon which can partly contribute to the lower reflectances of conifer-dominated areas. Other explanations include, for example, that the tree crown surface of coniferous stands is more heterogeneous than in broadleaved stands (Häme, 1991; Schull et al., 2011). In other words, when surface roughness (i.e. crown-level clumping) increases, the shaded area within the canopy increases, thus leading to lower reflectances. Overall, these results highlight the importance

of various geometric properties as the main reason for the reflectance differences between broadleaved and coniferous stands.

Remote sensing of the biophysical properties, such as LAI, of a boreal coniferous forest canopy layer is further complicated by the often dominating role of the understory in the spectral signal (Rautiainen et al., 2011; Rautiainen et al., 2007; Eriksson et al., 2006; Eklundh et al., 2001; Chen & Cihlar, 1996; Spanner et al., 1990). Coniferous forests that are regularly treated according to forest management practices tend to have relatively clumped and open canopies. Thus, the role of the understory vegetation in forming boreal forest reflectance cannot be neglected (Pisek et al., 2011).

1.3 Vegetation indices in LAI estimation

Canopy biophysical variables, such as LAI, can be estimated from remotely sensed data by two types of algorithms: empirical models and methods that use physically-based radiative transfer (RT) models. In empirical algorithms, the estimation is based on statistical relationships modelled between concurrent ground reference measurements and surface reflectance data. These relationships are typically expressed in the form of vegetation indices (VI). VIs include various combinations of spectral bands designed to maximize the sensitivity to vegetation characteristics while minimizing it to atmospheric conditions, background, view and solar angles (Baret & Guyot, 1991; Myneni et al., 1995). Operational LAI algorithms at global-scale typically make use of RT models, but the empirical models usually outperform them in more localized applications.

The design of a VI that is optimally correlated with a particular vegetation property requires good physical understanding of the factors affecting the spectral signal reflected from vegetation. The sensitivity of a VI to a vegetation characteristic is typically maximized by including bands with high sensitivity (e.g. high absorption) to the monitored entity and bands mostly unaffected by the same entity. The simplest forms of VIs are simple differences ($R_{B1}-R_{B2}$), ratios (R_{B1}/R_{B2}) and normalized differences [$(R_{B1}-R_{B2})/(R_{B1}+R_{B2})$] of the reflectances of two spectral bands (R_{B1} , R_{B2}). (In Table 2 we give examples of common VIs used in this study.) The most apparent characteristic of the green vegetation spectrum is the pronounced difference between the red and NIR reflectances, the so called red-edge around 700 nm. For example, the normalized difference vegetation index (NDVI) utilizes this difference and has been shown to correlate with many interrelated vegetation attributes, such as chlorophyll content, LAI, fractional cover, fAPAR and productivity.

The most commonly used VIs were designed for broadband sensors (one spectral band spans about 50 nm or more) having red and NIR bands, such as NOAA AVHRR and Landsat MSS (e.g. Tucker, 1979). However, the basic VIs in red and NIR spectral range suffer from three well-known problems in LAI estimation: (1) they are not sensitive to LAI over its natural range but tend to saturate already at moderate levels of LAI, (2) they are sensitive to canopy background variability, and (3) the VI-LAI relationships are dependent on the vegetation type. These VIs are also sensitive to atmospheric noise and correction.

The saturation of NDVI occurs typically at LAI levels of 2 to 6 depending on the vegetation type and environmental conditions (e.g. Sellers, 1985; Myneni et al., 1997). In general, NDVI saturates as the fractional cover of vegetation approaches one, although LAI still increases (e.g. Carlson & Ripley, 1998). Over conifer-dominated boreal forests, NDVI varies typically

in a narrow range and shows poor relationships with canopy LAI (Chen & Cihlar, 1996; Stenberg et al., 2004). The reason for this is the green understory, which results in a non-contrasting background in the visible part of the spectrum (Nilson & Peterson, 1994; Myneni et al., 1997).

Many modifications of basic VIs have been suggested to give better sensitivity to LAI. Typical modifications use other visible bands than red (e.g. the green vegetation index, GNDVI, Gitelson et al., 1996), try to reduce soil effects based on the soil line concept (e.g. the soil adjusted vegetation index, SAVI, Huete, 1988), or include short wave infrared (SWIR) bands. Many modifications also attempt to reduce atmospheric effects (e.g. the enhanced vegetation index, EVI, Huete et al., 2002). The soil line is based on the observation that soil reflectances fall in a line in the red-NIR spectral space (e.g. Huete, 1988). Many VIs utilize the parameterized soil line in their calculation, but these VIs have not been successful in boreal forests as bare soil is rarely visible (e.g. Chen, 1996).

The sensitivity of shortwave infrared (SWIR) reflectance to forest biophysical variables has been recognized for a long time (e.g. Butera, 1986; Horler & Ahern, 1986) and several VIs utilizing the SWIR band have been designed. Rock et al. (1986) showed that the moisture stress index (MSI), i.e. the ratio of SWIR reflectance to NIR reflectance, was an indicator of forest damage. Later, the ratio has commonly been referred to as the infrared simple ratio (ISR, Chen et al., 2002; Fernandes et al., 2003). The SWIR reflectance has also been used for adjusting NDVI (Nemani et al., 1993) and SR (Brown et al., 2000). The reduced simple ratio (RSR) has been used specifically for estimating LAI (Brown et al., 2000; Stenberg et al., 2004) and has been employed also in regional and global-scale operational algorithms (Chen et al., 2002; Deng et al., 2006). RSR seems to reduce the sensitivity to the type and amount of understory vegetation, because background reflectance varies less in SWIR than in visible and NIR (Brown et al., 2000; Chen et al., 2002). RSR has also some capability to unify coniferous and broadleaved forest types, which reduces the need for land cover type specific LAI algorithms. However, in comparison to ISR, the use of red band makes RSR sensitive to atmospheric effects (Fernandes et al., 2003). However, although inclusion of SWIR reflectance increases the sensitivity of VIs to LAI, these indices also have a tendency to saturate at high levels of LAI (e.g. Brown et al., 2000; Heiskanen et al., 2011).

Imaging spectroscopy provides much narrower spectral bands than typical multispectral sensors. Due to the more detailed sampling of the vegetation spectra, such data can detect specific absorption features of vegetation and therefore improve the estimation of vegetation biochemical properties. For example, the SPOT 5 HRG sensors capture a spectral range from 500 nm to 1750 nm with four broad bands, in comparison to Hyperion's 242 (10 nm wide) bands between 400 nm and 2500 nm. At the canopy scale, the contents of biochemical components and LAI are highly inter-related (e.g. Asner, 1998; Roberts et al., 2004). Therefore, imaging spectroscopy could potentially improve LAI estimates. Furthermore, there is potentially complementary information outside the typical spectral bands of broadband sensors.

One way to utilize imaging spectroscopy data is to calculate narrow-band VIs in a similar fashion as for broadband data but using narrower bands. The aim is to improve the sensitivity of the VI to a specific vegetation biochemical property. For example, Ustin et al. (2009) give a comprehensive review on VIs used as indicators of plant pigments (chlorophyll, carotenoids and anthocyanin). The methods of estimating the non-pigment

biochemical composition of vegetation (water, nitrogen, cellulose and lignin), on the other hand, are reviewed by Kokaly et al. (2009). Many of the developed indices have been designed to work at leaf level and do not necessarily upscale to canopy level, because of the high sensitivity to canopy structure, background, solar and view geometry. Another approach is to find iteratively the simple combinations of bands that give the best correlation with empirical data (e.g. Mutanga & Skidmore, 2004; Schlerf et al., 2005).

Most chlorophyll indices exploit the information in the red edge around 700 nm (Ustin et al., 2009). Imaging spectroscopy data also enables the estimation of the red edge position (REP), which is particularly sensitive to changes in chlorophyll content (e.g. Dawson & Curran, 1998). Water indices, on the other hand, utilize the water absorbing regions in the SWIR region of the spectrum (e.g. Gao, 1996; Zarco-Tejada et al., 2003). Those indices seem particularly interesting for LAI estimation considering the importance of the SWIR spectral region in estimating LAI using broadband indices.

There is growing evidence that imaging spectroscopy data can improve LAI estimates in comparison to broadband data by reducing the saturation effects. Depending on the vegetation type and range of LAI, different types of VIs have been found useful. However, the red edge indices have been most effective in estimating LAI of crops (Wu et al., 2010), grasslands (Mutanga & Skidmore, 2004) and thicket shrubs (Brantley et al., 2011). On the other hand, indices based on NIR and SWIR bands have been successful in broadleaved (le Maire et al., 2008) and coniferous forests (Gong et al., 2003; Schlerf et al., 2005; Pu et al., 2008). The importance of the SWIR spectral region in estimating boreal forest LAI has also been emphasized by multivariate regression analysis (e.g. Lee et al., 2004). However, broadband sensors can also have advantages over narrowband sensors in LAI estimation, for example, by being less sensitive to noise due to the sensor, atmosphere and background (e.g. Broge & Leblanc, 2000). Although there are case studies from different biomes, the performance of narrowband VIs has been poorly assessed over European boreal forests.

2. Case study

2.1 Aims

The aim of the study is to establish the extent to which vegetation indices can be used to measure variation in LAI based on a test site in southern boreal forest in Finland. We explore different VIs in LAI estimation during full leaf development. We compare the performance of narrowband VIs to traditional broadband VIs. The objective is to identify VIs, which are least sensitive to species composition and, on the other hand, perform well in coniferous stands.

2.2 Materials and methods

2.2.1 Study area

The study area, Hyytiälä, is located in the southern boreal zone in central Finland (61° 50'N, 24°17'E) and has an annual mean temperature of 3°C and precipitation of 700 mm. Dominant tree species in the Hyytiälä forest area are Norway spruce (*Picea abies* (L.) Karst), Scots pine (*Pinus sylvestris* L.) and Silver birch (*Betula pendula* Roth). Understory vegetation, on the other hand, is composed of two layers: an upper understory layer (low dwarf shrubs

or seedlings, graminoids, herbaceous species) and a ground layer (mosses, lichens). The growing season typically begins in early May and senescence in late August. We measured twenty stands from the Hyytiälä forest area in July 2010 (see Section 2.2.2, Table 1). The stands represented different species compositions that are typical to the southern boreal forest zone in Finland.

Site	Vegetation	Site type	Tree height, m	Basal area, m ² /ha	LAI
A4	Pine	mesic	15.8	20.4	1.77
A5	pine, understory broadleaf	mesic	18.6	24.3	2.67
B2	spruce, understory birch	mesic	7.5	10	2.64
D3	pine, understory spruce & birch	sub-xeric	17.8	20.5	2.37
D4	spruce, 25% birch	mesic	16.5	27.5	3.72
E1	birch, spruce understory	mesic	19.1	10.7	2.58
E5	50% spruce, 50% birch	mesic	23.1	27.2	4.12
E6	50% spruce, 40% birch, 10% pine	mesic	10.2	22.2	3.34
E7	Spruce	mesic	13.3	31.7	3.91
F1	birch, spruce understory	mesic	13.8	20.9	3.37
G4	spruce, 15% birch, 10% pine	herb-rich	15.5	29.1	4.57
H3	Birch	herb-rich	14.9	10.7	2.63
H5	Birch	herb-rich	14.1	20.6	2.77
I4	birch, understory pine, spruce seedlings	mesic	2.4	4	2.61
T	Spruce	mesic	24.6	56	3.43
U16	Birch	mesic	14	21	2.69
U17	birch, 10% spruce	herb-rich	11.7	27	3.35
U18	65% pine, 25% spruce, 10% birch	sub-xeric	16.5	26	3.45
U26	20% pine, 70% spruce, 10% birch	mesic	16.8	24.9	2.43
U27	5% pine, 90% spruce, 5% birch	mesic	15.2	20.9	2.63

[pine = Scots pine, spruce = Norway spruce, birch = Silver birch]

Table 1. Study stands.

2.2.2 Ground reference measurements

The LAI-2000 Plant Canopy Analyzer (PCA) is one of the most commonly used optical devices to measure LAI. The PCA's optical sensor includes five concentric rings of different zenith angles (θ) (together covering almost a full hemisphere), which measure diffuse sky

radiation between 320-490 nm (LI-COR, 1992). Measurements by the PCA performed below and above the canopy yield canopy transmittances, $T(\theta)$, for each ring. Finally, LAI is calculated by numerical approximation of the integral (Miller, 1967):

$$LAI = -2 \int_0^{\pi/2} \ln[T(\theta)] \cos\theta \sin\theta d\theta \quad (1)$$

There are four fundamental assumptions behind the LAI calculation method: 1. leaves (needles) are optically black in the measured wavelengths (implying that canopy transmittance closely corresponds to canopy gap fraction), 2. leaves (needles) are randomly distributed inside the canopy volume, 3. leaves (needles) are small compared to the area of view of the PCA's rings, and 4. leaves (needles) are azimuthally randomly oriented. The LAI estimate produced by Eq. 1 is commonly called effective LAI as the foliage elements are not randomly organized but typically clumped (or grouped) together, which causes the estimate produced by the PCA to be smaller than the "true" LAI (Chen et al., 1991; Deblonde et al., 1994).

The LAI measurements can be done either with one or two PCA instruments. One PCA is used for small plants such as crops, but for taller plants (e.g. trees), two units are necessary. When only one instrument is used, the measurement is at first taken below and then above the canopy. If two instruments are used, one instrument remains above the canopy and the other one below the canopy. The use of two instruments is preferable since data are logged nearly simultaneously with both sensors. The LAI estimate is calculated by combining below and above canopy data. The measurements should be conducted under diffuse light conditions; for example, when the sky has a full cloud cover or the sun angle is low (less than 16 degrees). The radius of the sample plot should be at least three times the dominant tree height as the PCA instrument has a relatively large opening angle.

In this study, the ground reference LAI (Table 1) was acquired by operating two LAI-2000 PCA instruments simultaneously. The instruments were intercalibrated before measurements were performed. The reference sensor was located above the forest canopy and set at a 15-second logging interval, while the other sensor was used inside the forest. The sampling scheme was a 'VALERI-cross' (Validation of Land European Remote Sensing Instruments, VALERI) which consists of two perpendicular 6-point transects. The distance between two measurement points was four meters, so that the sampling scheme corresponded roughly to a 20 m x 20 m plot. Measurement height was kept constant at 0.7 meters.

2.2.3 Satellite data

In this study, we used narrowband spectral data obtained from a Hyperion satellite image. Hyperion is a narrowband imaging spectrometer aboard the National Aeronautics and Space Administration (NASA) Earth Observer-1 (EO-1) satellite launched in 2000. Hyperion captures data in the 'pushbroom' manner in 7.7 km wide strips using 242 spectral bands. The spectral range of Hyperion is 356-2577 nm with each band covering a nominal spectral range of 10 nm. Each pixel in a Hyperion image corresponds to an area of 30 m x 30 m on the ground. During an acquisition, a scene with a length of either 42 km or 185 km is recorded. Hyperion is in a repetitive, circular, sun-synchronous, near-polar orbit at an

altitude of 705.3 km measured at the equator. Thus, it can image almost any point on Earth and it flies over all locations at approximately the same local time. The nominal revisit time is 16 days, but due to the possibility of tilting the sensor, the potential revisit frequency is higher. The scene used in this study was captured on 03 July 2010, and was provided courtesy of the U.S. Geological Survey (USGS) Earth Explorer service.

Out of the potential 242 spectral bands, several lack illumination (due to the absorption in the atmosphere or a decrease of incident solar spectral irradiance in the longer infrared wavelengths) or have a very low spectral response. This leaves the user with 198 usable spectral bands: bands 8-57 in the visible and NIR (wavelengths 436-926 nm) and bands 77-224 in SWIR (wavelengths 933-2406 nm) (Pearlman et al., 2003). Hyperion images have several known deficiencies which can be corrected using algorithms given in scientific literature. Firstly, Hyperion suffers from systematic striping in along-track direction of the image. The stripes are characteristic to all pushbroom sensors. Instruments belonging to this broad class have a different receiving element for each image line. Hyperion has thus 256 radiation-sensitive elements for each spectral band, each seeing a separate 30 m strip of the ground, thus producing the 7.7 km wide image. The striping can be broadly divided into two classes, completely missing lines (due to non-functioning receiving elements) and actual stripes (arising from slightly different sensitivities of the 256 receivers). We removed the actual striping using Spectral Moment Matching (SpecMM), outlined by Sun et al. (2008), which uses the average and standard deviation statistics between highly correlated bands to remove stripes. Next, the missing lines containing no information were identified and corrected using the values from spatially adjacent pixels using local destriping (Goodenough et al., 2003). The results of the destriping can be seen in Figure 1.

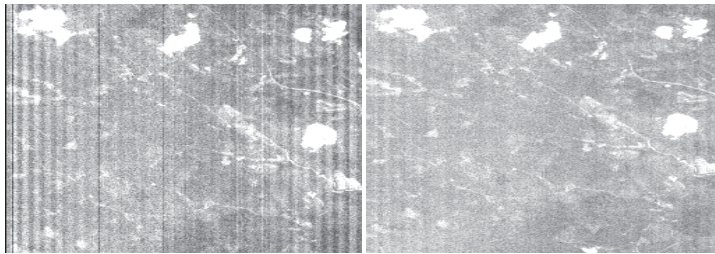


Fig. 1. Hyperion band 8 (436nm) uncorrected image (left), and corrected using Spectral Moment Matching and local destriping (right).

The second known defect in Hyperion imagery is a shift in the wavelength of each column in the across track direction from the band central wavelength. This shift, known as spectral smile, is also characteristic to pushbroom sensors and is a result of different optical paths leading to the different receiving elements. The shift is a function of wavelength and the position of the receiving element in the receiving array. As is the case for most instruments, the “smile” manifests itself in Hyperion imagery as a “frown”, with the wavelengths of the columns near the edges of each band shifting negatively from the bands average wavelength (Figure 2). The smile was corrected using the pre-launch laboratory measured spectral shift (Barry, 2001). We used interpolation to bring each individual pixel to a common central wavelength based on the pre-launch calibration measurements.

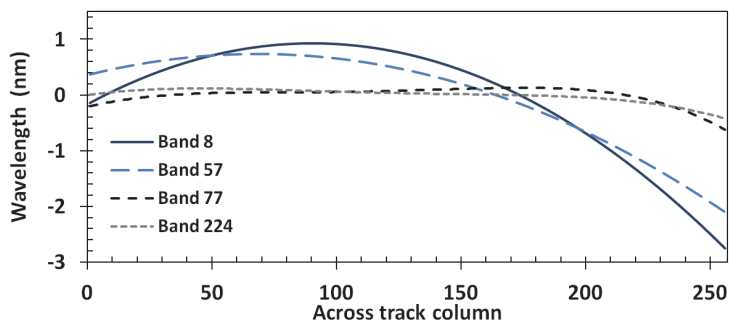


Fig. 2. Laboratory measured spectral shift of Hyperion (Barry, 2001).

The signal received by the Hyperion instrument consists of the photons scattered by the atmosphere as well as the ground surface. To study surface reflectance, the influence of the atmosphere needs to be eliminated in a process commonly known as atmospheric correction. We performed this correction using an algorithm known as Fast Line-of-sight Atmospheric Analysis of Spectral Hypercubes (FLAASH, Matthew et al, 2000). FLAASH is an absolute atmospheric correction that incorporates the MODTRAN4 radiation transfer code to model the scattering and transmission properties of the atmosphere at the time of image capture (San & Suzen, 2010). The FLAASH algorithm is incorporated into the ITT Visual Information Solutions (ITT VIS) ENVI software. For processing, FLAASH requires an input value for visibility to estimate atmospheric aerosol levels, in addition to basic geographic and temporal details about the scene. The visibility can be recalculated by FLAASH, using a ratio between dark pixels at 600 nm and 2100 nm. However, a more accurate estimate of visibility was achieved using ground based optical measurements from a weather station in the area.

The final processing stage is to resample the image pixels into a geographic coordinate system, known as geocorrection. This was done using a polynomial transformation to a vector base map from the National Land Survey of Finland. The Hyytiälä area contains numerous roads, providing a large number of easily identifiable potential ground control points (GCPs) at intersections. Around 20 GCPs were selected, with a root mean square error of 0.4 pixels being achieved. Bilinear interpolation was chosen for resampling the image pixels due to the better geometric accuracy over nearest neighbour.

The final product is a geocorrected image of the surface hemispherical-directional reflectance factors (HDRF) of the Hyytiälä area. To validate the atmospheric correction, we compared the HDRF to a field measured reflectance factor. A soccer field of about 130 m by 60 m in the area was sampled during the summer of 2010 every two to three weeks using an ASD handheld portable spectroradiometer covering a spectral range from 325-1075 nm. The sampling was done using a transect approach with 42 measurements at around 1 meter intervals. The final hemispherical-conical reflectance factor (HCRF) used for the comparison is an average of the transect representing the average for the whole field. While no ground measurements fell on the exact date of the Hyperion image, the ground measured spectra was interpolated to dates between two measurements. After interpolation the ground measured HCRF was binned into corresponding Hyperion bands using the spectral response of each band.

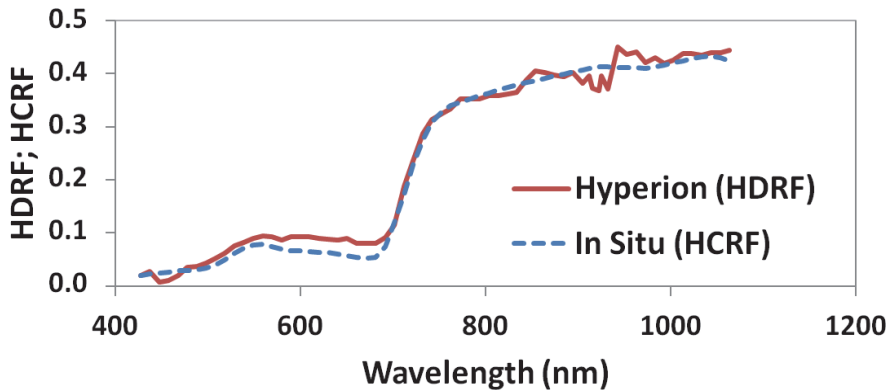


Fig. 3. Comparison of a soccer field's spectral reflectance factors from in situ radiometric measurements and corrected Hyperion data.

Overall, there is a very good correlation between the field measured reflectance and the fully processed Hyperion reflectance (Fig. 3). An overall RMSE of 1.8% is achieved, which gives us confidence in the validity of the pre-processing and atmospheric correction. However, as the *in situ* spectrum is considerably smoother than the one measured from the satellite, a considerable amount of noise is also present in the satellite-derived HDRF.

2.2.4 Vegetation indices and statistical analysis

First, we studied how HDRFs in single bands are correlated with LAI. Next, in order to evaluate narrow-band VIs for estimating LAI, we did regression analyses between various VIs and LAI. We used two approaches to select narrowband indices: 1) We made a literature survey for narrow-band VIs that have been designed to estimate foliage biochemical components. (A collection of VIs showing the highest R^2 with LAI are shown in Table 2.) 2) We calculated all the possible Ratio Indices (RI) and Normalized Difference Indices (NDI) of Hyperion bands and correlated them with LAI. In other words, the first approach also contains VIs combining several bands and the second approach aims to identify the simple two-band VIs that best correlate with LAI.

To facilitate the comparison of narrowband VIs with broadband indices, we calculated synthetic HDRFs based on Landsat 7 ETM+ bands. The HDRFs were calculated according to Jupp et al. (2002) using the ETM+ spectral sensitivity functions, and Hyperion's central wavelengths and bandwidths. Four broadband indices were calculated for comparison, SR, NDVI, ISR and RSR (Table 2). All these indices have been used for LAI estimation in various biomes. SR and NDVI were included for reference, and ISR and RSR because they have shown best performance over conifer-dominated boreal forests (see 1.3).

We analyzed the data both by grouping all the sample plots together and separately for coniferous plots (> 75% of the trees were Scots pines or Norway spruces). In the birch-dominated stands, the variation in LAI was too small for reliable regression analysis.

We studied only linear relationships. The strength of the relationship was assessed by the coefficient of determination (R^2) and the root mean square error (RMSE).

Abbr.	Index	Formula	Reference	Bands applied
Indices concentrating on the red-edge				
SR	Simple Ratio	$SR = R_{ETM+4}/R_{ETM+3}$	Rouse et al. (1974), Birth & McVey (1968)	ETM+3, ETM+4
NDVI	Normalized Difference Vegetation Index	$NDVI = (R_{ETM+4} - R_{ETM+3}) / (R_{ETM+4} + R_{ETM+3})$	Rouse et al. (1974)	ETM+3, ETM+4
REP	Red Edge Position	$REP = 700 + (((R_{773} + 1,5 * R_{662}) - R_{692}) / (R_{733} - R_{692})) * (740 - 700)$	Danson & Plummer (1995)	773, 662, 692, 733
Indices concentrating on pigment content				
PSSRa	Pigment-Specific Simple Ratio - chl _a	$PSSRa = R_{803}/R_{681}$	Blackburn (1998)	681, 803
Water sensitive indices				
MSI = ISR	Moisture Stress Index = Infrared Simple Ratio	$ISR = R_{ETM+5}/R_{ETM+4}$	Rock et al. (1986), Fernandes et al. (2002)	ETM+4, ETM+5
RSR	Reduced Simple Ratio	$RSR = (R_{ETM+4}/R_{ETM+3}) * ((R_{ETM+5_min} - R_{ETM+5}) / (R_{ETM+5_max} - R_{ETM+5_min}))$	Brown et al. (2000)	ETM+3, ETM+4, ETM+5

Table 2. Vegetation indices investigated in this study. The symbol R refers to the HDRF. Subscripts refer to the applied ETM+ band or the central wavelength (in nm) of the Hyperion band

2.3 Results

2.3.1 General characteristics of forest spectra

Two examples of forest reflectance factors (HDRFs) are presented in Figure 4. To allow relating the vegetation spectra to satellite signals, the sensitivity functions of the corresponding ETM+ bands are shown. Note the correspondence of ETM+2 with the green peak, ETM+3 with the red local minimum and ETM+4 with the plateau in the NIR. The red-edge slope (between ETM+ bands 3 and 4) is not covered by ETM+ bands. ETM+5 and ETM+7 catch the signal in the shortwave infrared region (SWIR-1 (here: 1470-1800 nm) and SWIR-2 (here: 2030-2360 nm) respectively), avoiding the two strong water absorption bands in-between.

The average reflectance of coniferous stands is slightly lower in the green region and decidedly lower in the NIR than the reflectance of birch stands. In SWIR-1 (covered by ETM+5) the reflectances become more comparable, and in SWIR-2 (covered by ETM+7) the signals almost meet.

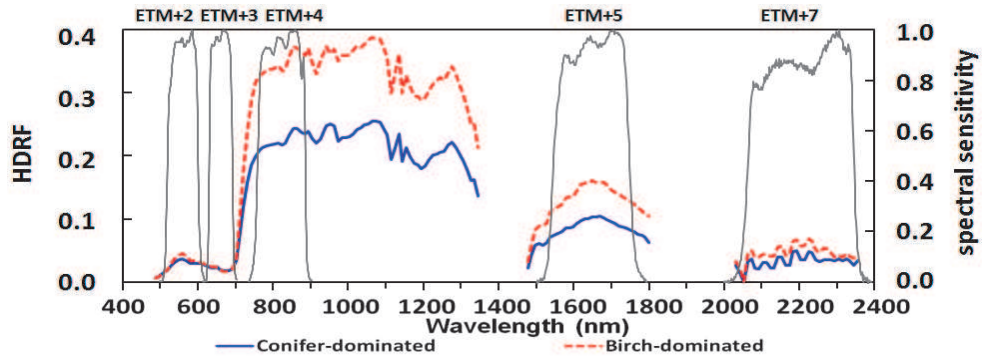


Fig. 4. Average conifer and birch-dominated stand spectra. The grey lines show the spectral sensitivity of the ETM+ bands.

2.3.2 Regression analysis for single bands

The different average HDRF for the two forest types (Fig. 4) results in different correlations of the satellite bands to LAI (Fig. 5).

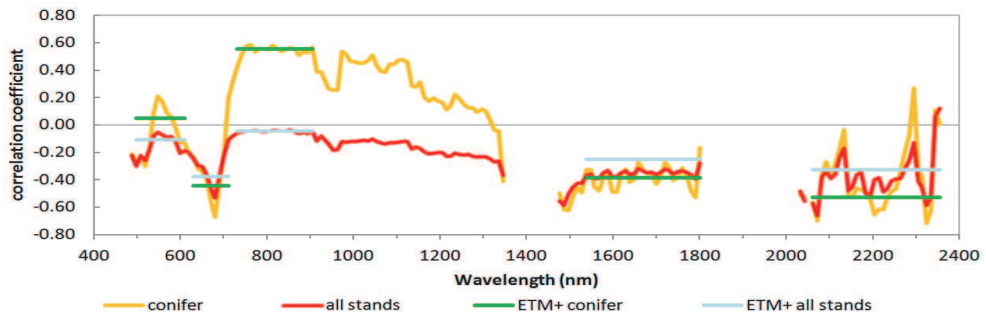


Fig. 5. Correlation coefficient of LAI with ETM+ and Hyperion spectral bands for all sample stands, and separately for conifer sample stands.

The correlation coefficients for all stands varied between -0.6 and -0.038. All correlations were negative, except for the two Hyperion bands centred at 2345 nm and 2355 nm. Two important regions (green and NIR) had almost no correlation with LAI. Only the absorption peak of chlorophyll produced a strong negative correlation at 681 nm. The SWIR correlations were also mostly negative.

For conifer stands, correlation coefficients varied between -0.7 and 0.6. The first peak was at 549 nm, in the middle of the green band, followed by a strong negative correlation in the red with a peak at 681 nm. In the NIR a strong positive correlation was observed again. A slight shoulder began at 712 nm, with a plateau at 752 nm. In the SWIR, correlation coefficients were very close to those of all stands.

Fig. 5 also shows the correlation of the ETM+ bands to LAI. The lower spectral resolution averages wider wavelength ranges and therefore shows less variation in correlation coefficients.

2.3.3 Correlation of vegetation indices to LAI for all sample plots

The best broadband index analysed here was the Infrared Simple Ratio (ISR, $R^2 = 0.56$), followed by the Reduced Simple Ratio (RSR, $R^2 = 0.40$) (Table 3). The best narrowband combinations (either RI or NDI) showed more potential with R^2 s exceeding 0.65 (Table 3, Fig. 6). If there were several indices based on neighbouring bands (within 10 nm) we chose the best one to Table 3.

VI	Bands applied	R^2	RMSE	RMSE Conifer	RMSE Broadleaf
broadband indices using simulated ETM+					
ISR	ETM+4, ETM+5	0.56	0.44	0.42	0.25
RSR	ETM+3, ETM+4, ETM+5	0.40	0.52	0.59	0.31
NDVI	ETM+3, ETM+4	0.09	0.64	0.68	0.51
SR	ETM+3, ETM+4	0.04	0.66	0.73	0.46
narrowband indices using Hyperion					
RI	1134, 1790	0.71	0.36	0.34	0.38
NDI	1134, 1790	0.68	0.38	0.36	0.39
RI	732, 1790	0.67	0.38	0.42	0.31
RI	1074, 1790	0.67	0.38	0.40	0.34
RI	885, 1790	0.67	0.39	0.37	0.35
RI	854, 1790	0.66	0.39	0.37	0.34
RI	1003, 1639	0.66	0.39	0.39	0.26
RI	1044, 1790	0.66	0.39	0.39	0.37
NDI	732 1790	0.66	0.39	0.42	0.33
NDI	1084, 1286	0.66	0.39	0.43	0.22

Table 3. Indices most correlated with LAI for all sample plots. RMSE was also calculated separately for each forest class. Bands for Hyperion refer to the central wavelength (in nm).

The best band combinations for RI and NDI indices were very similar (Fig. 6). A strong correlation with LAI existed for bands combining the region between 730 to 900 nm and 1130 to 1350 nm. Another interesting region was within SWIR-1; especially strong was the correlation around 1780 and 1790 nm. These bands also showed up in the best performing indices for all forest classes combined (Table 3).

The two best narrowband indices for all forest plots were the RI ($R^2 = 0.71$, RMSE = 0.36) and NDI ($R^2 = 0.68$, RMSE = 0.38) based on bands centred at 1134 and 1790 nm (Table 3). This is consistent with the best broadband index (ISR) which also combines NIR and SWIR. The same spectral regions are used by all the other best indices except two cases including a band in the red-edge (732 nm). Examples of the strongest relationships are shown in Fig. 7. However, when looking at the RMSE for conifer and broadleaf stands (Table 3) it became apparent that for some indices (e.g. NDI based on 1084 nm and 1286 nm: RMSE = 0.43 for conifers and RMSE = 0.22 for broadleaf) their LAI was correlated differently to the same VI.

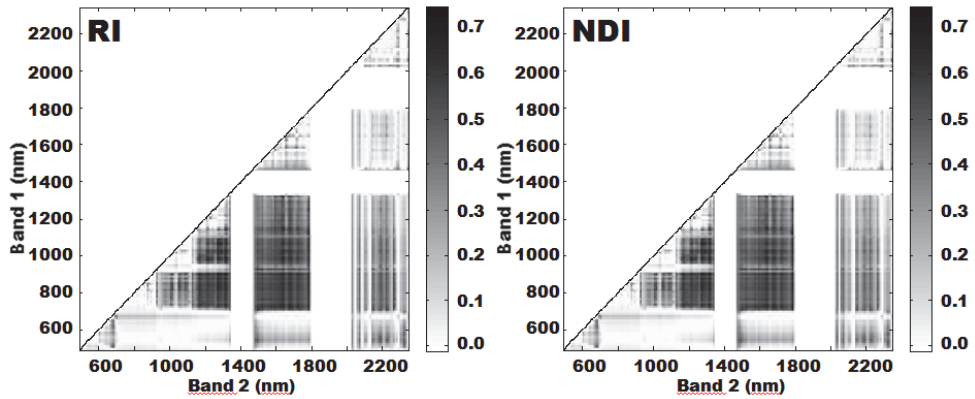


Fig. 6. Matrixes showing the R^2 between LAI and simple narrowband indices calculated for all possible combinations of Hyperion bands. The indices are defined as follows: $RI = \text{Band1}/\text{Band2}$, and $NDI = (\text{Band1} - \text{Band2}) / (\text{Band1} + \text{Band2})$.

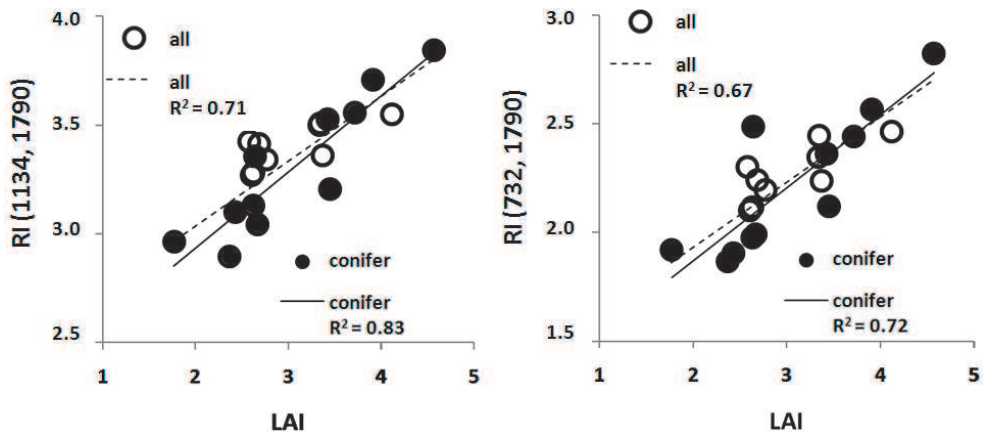


Fig. 7. The relationship of LAI and two best ratio indices (RI).

2.3.4 Correlations for coniferous dominated forest plots

The performance of the broadband indices for conifer-dominated stands was much better than over all sample stands. R^2 now ranged from 0.60 to 0.79, and NDVI showed the best correlation with LAI, followed by SR.

The best performing narrowband index over coniferous forest was neither RI nor NDI but REP ($R^2 = 0.89$) calculated according to the method of Danson & Plummer (1995) (Table 2). This index combined four bands in the visible and NIR; an area also represented in several of the other indices which best correlated with LAI in coniferous stands.

The matrixes for all band combinations of Hyperion bands over conifer-dominated stands (Fig. 8) showed wider spectral regions of high correlation than for all stands (Fig. 6).

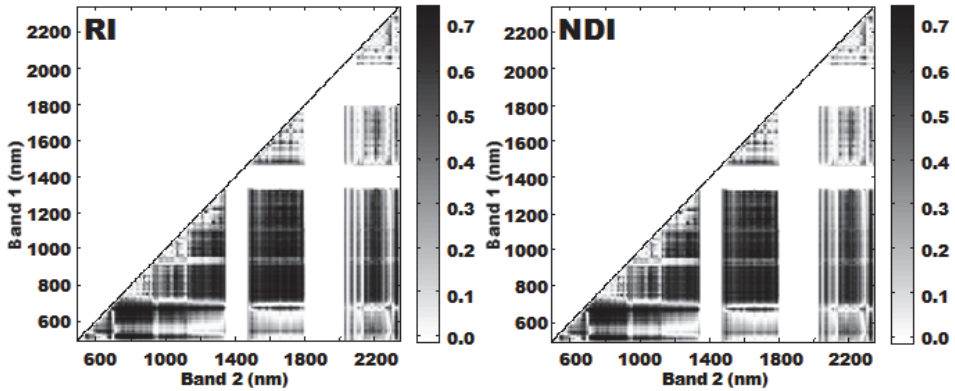


Fig. 8. Matrixes showing the R² between LAI and two narrowband indices calculated for all possible combinations of Hyperion bands for conifer-dominated stands.

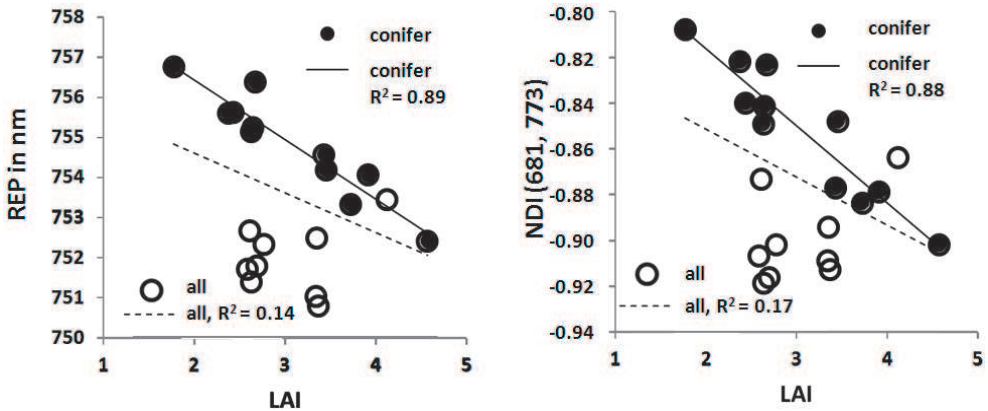


Fig. 9. The relationship of LAI and the two best performing narrowband indices for conifer-dominated stands.

Most of the indices with the highest correlations to LAI in coniferous stands used bands around the red-edge. Almost all of them (e.g. the Pigment-Specific Simple Ratio Index for chlorophyll a, PSSRa) applied the Hyperion band centred at 681nm, the peak of chlorophyll a absorption. Exceptions were the RI and NRI using the bands centred at 1185 and 1790 nm (i.e. combining NIR and SWIR), and RI and NDI using bands centred at 518 and 773 nm (i.e. combining carotene absorption and NIR).

Scatterplots for the two best indices for coniferous stands are shown in Fig. 9. In both cases, coniferous plots differed considerably from the other plots. This was indicated also by the high RMSE for all stands (up to 1.42, Table 4). However, for indices using NIR and SWIR (e.g. RI and NDI based on 1185 and 1790 nm) the differences were less pronounced. The VI showing the lowest RMSE for all stands (0.49) was the RI (1185 and 1790 nm) with an R² for conifer stands of 0.86 and RMSE 0.29.

VI	Bands applied	R ²	RMSE	RMSE All stands
broadband indices using simulated ETM+				
NDVI	ETM+3, ETM+4	0.79	0.36	1.20
SR	ETM+3, ETM+4	0.78	0.36	1.56
ISR	ETM+4, ETM+5	0.71	0.42	0.44
RSR	ETM+3, ETM+4, ETM+5	0.60	0.50	0.90
narrowband indices using Hyperion				
REP	671, 702, 742, 783	0.89	0.26	1.29
NDI	681, 773	0.88	0.27	1.02
RI	681, 773	0.88	0.28	1.01
RI	1185, 1790	0.86	0.29	0.49
NDI	1185, 1790	0.86	0.30	0.50
NDI	681, 742	0.85	0.30	1.01
NDI	681, 824	0.85	0.30	0.98
RI	681, 742	0.85	0.31	0.99
NDI	518, 773	0.85	0.31	1.42
PSSRa	803, 681	0.85	0.31	1.30
RI	518, 773	0.85	0.31	1.39

Table 4. Indices most correlated with LAI in conifer-dominated plots. R² and RMSE for conifer-dominated stands, and RMSE separately for all stands. Bands for Hyperion refer to the central wavelength (in nm).

2.4 Discussion

In our case study, the narrowband VIs provided more accurate LAI estimates than the broadband VIs synthesized from the same data in a boreal forest study site. The best narrowband combinations showed relatively strong linear relationships with LAI ($R^2 > 0.65$), although the Hyperion image was acquired in the middle of the growing season when LAI is the highest. The relationships were even stronger if the analysis was restricted to the conifer stands ($R^2 > 0.85$). The results are promising as common broadband VIs tend to saturate at the highest LAI values. The improvement of estimation accuracy is in agreement with the previous studies, which have emphasized the potential of narrowband VIs for estimating forest canopy LAI (e.g. Lee et al., 2004; Schlerf et al., 2005; Brantley et al., 2011; Wu et al., 2010).

Most of the narrowband VIs showing the strongest relationships with LAI were based on reflectances in the far red and at the red edge (680–740 nm), NIR (e.g. 885 and 1134 nm) and SWIR (e.g. 1639 nm and 1790 nm) wavelength regions (Figure 10). Many of the most important spectral regions are not covered by the ETM+ spectral bands, and the spectral regions are very narrow in comparison to the ETM+ bands.

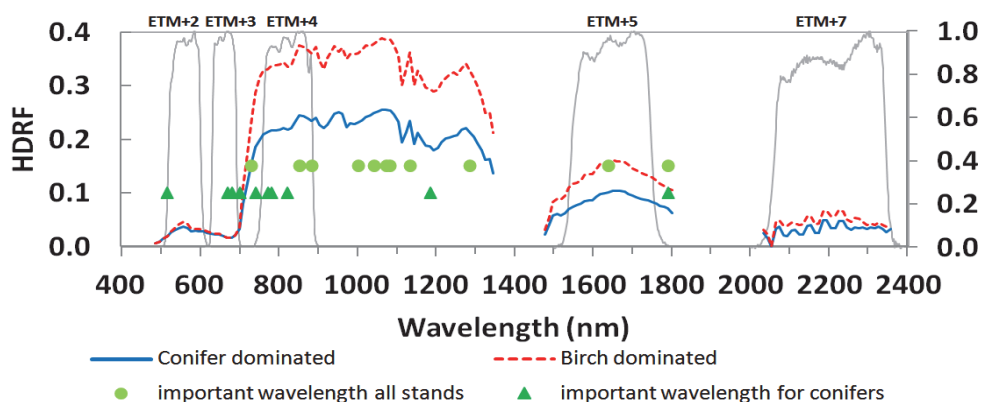


Fig. 10. Spectral regions used by the indices showing the strongest relationships with LAI over all sample stands and conifer stands.

The NIR and SWIR spectral bands were particularly important when all sample plots were analyzed together. This is in agreement with the best broadband indices, ISR and RSR. The importance of NIR and SWIR bands has been emphasized also in previous studies testing narrowband VIs for estimating forest LAI (e.g. Lee et al., 2004; Schlerf et al., 2005). The leaf (needle) reflectance at those wavelengths is mainly controlled by water absorption, although leaf biochemical components such as proteins, cellulose and lignin also contribute to absorption in the infrared (e.g. Curran, 1989). The amount of water at the canopy level is directly related to LAI, which explains strong correlations. The bands centered at 1134 nm and 1790 nm are among the Hyperion bands, which are closest to the water absorption regions centered at approximately 1200 nm and 1940 nm. The spectral bands close to the water absorption regions at 970 nm and 1400 nm are also employed in some of the best indices. The spectral bands of the broadband sensors are usually placed in the middle of the atmospheric windows to avoid atmospheric absorption. However, it seems that narrow spectral bands close to the water absorption regions are particularly interesting for estimating LAI. In these wavelength regions, the reflectance seems to be relatively insensitive to tree species or composition of the understory vegetation, as suggested earlier by the studies using broadband indices (e.g. Brown et al., 2000).

When pure coniferous stands were studied separately, the relationships became stronger and the far red and red edge spectral bands were included in several of the best VIs. However, the improvement in accuracy relative to the best VI based on NIR and SWIR reflectance (RI based on bands centered at 1185 nm and 1790 nm) was rather modest. The best broadband indices were NDVI and SR, which are based on ETM+ red and NIR bands. Usually, NDVI has shown relatively weak relationships with LAI in conifer dominated boreal forest (e.g. Stenberg et al., 2004).

The strongest relationship with LAI was provided by the red edge position (REP) calculated by the method proposed by Danson and Plummer (1995). In general, the REP is considered to be sensitive to leaf and canopy chlorophyll content, so that increasing the amount of chlorophyll, or LAI, is related to the longer REP wavelength because of the widening of the chlorophyll absorption region at approximately 680 nm (Danson & Plummer, 1995; Dawson

and Curran, 1998; Sims & Gamon, 2002; Pu et al., 2003). In comparison to SWIR spectral bands, the far red and red edge spectral region is sensitive to species composition, shown as poor relationships over mixed vegetation. However, sometimes poor relationships between the REP and LAI have been reported even for pure coniferous stands (Blackburn, 2002). However, although the REP calculated in this study showed strong correlation with coniferous LAI, the estimated wavelengths do not correspond to the Red Edge Inflection Point (REIP), i.e. the steepest slope of the red-edge. The wavelengths are considerably longer. Therefore, the unusual inverse relationship between REP and LAI in this study is explained by the calculation method (Danson and Plummer, 1995). Alternative calculation methods for REP are summarized, for example, by Pu et al. (2003).

Although many studies testing narrowband VIs for LAI estimation have stressed the potential of the red edge and SWIR spectral regions, the specific spectral bands providing the strongest relationships with LAI vary between the studies. Also in our case study, the optimal band combinations provided stronger relationships with LAI than VIs collected from the literature. This is somewhat expected, as the number of spectral bands and their possible combinations is so large that empirically determined optimal band combinations are likely to depend heavily on the local environmental conditions and type of satellite image data. For example, approximately 150 useful spectral bands of Hyperion make more than 20,000 two-band combinations. Because of this, the optimal indices cannot necessarily be generalized very well. Furthermore, a large number of spectral bands combined with a small number of sample plots increase the risk that the regression models are overfitted. However, this should be mostly a problem with multivariate approaches (e.g. Lee et al., 2004). Moreover, when comparing broadband and narrowband indices, it should be noted that we used only synthesized ETM+ data and the results could differ to some extent if true ETM+ data would have been used instead (Lee et al., 2004). This is because the synthetic broadband data is affected by the lower signal-to-noise ratio of the narrow spectral bands, even if data are averaged.

3. Future perspectives

Wider use of imaging spectroscopy data is hampered by the availability of the data. Today, mostly airborne instruments are used to produce remote sensing data with high spectral resolution. Airborne measurements are associated with relatively small spatial coverage and high operating costs falling directly to data users. The Hyperion sensor used in this case study is a rare exception: it is the only true imaging spectrometer in orbit today, providing wide spectral coverage with uniform spectral resolution and contiguous bands. The scene, however, is about to change. At the end of the decade (i.e., around 2020), NASA is planning to launch the HypSPIRI mission, providing narrowband data with routine global coverage (Samiappan et al., 2010). Before HypSPIRI, several national space programs are striving to launch satellites with capability to produce narrowband data (e.g. the EnMAP instrument, Segl et al., 2010). Therefore, the need for developing algorithms that would make use of the advanced properties of narrowband data, compared to the more traditional multispectral data, is evident.

In this case study, we used narrowband VIs to relate forest LAI to remotely sensed reflectance signals. Historically, vegetation indices have been among the very first tools in interpreting multispectral remote sensing data from vegetated areas. Later, physically-based

reflectance modelling has taken over the role of the preferred method in large-scale retrievals of vegetation biophysical variables. Similar developments may take place in the interpretation of narrowband imaging spectroscopy data. However, let us first take a closer look at narrowband indices as they are used in the current study.

As discussed above (section 1.3), VIs are usually treated as empirical (or, at least semi-empirical) tools in remote sensing. However, it has been known for a long time that the reflectance indices convey also some information on the physical processes related to the interaction of light with plant elements. Indeed, Myneni et al. (1995) showed that the common indices are actually derivatives of canopy reflectance and are physically related to abundances of absorbing pigments. For this reason, indices commonly make use of two spectral regions: one inside the spectral region where the absorption of a pigment is strong, and one outside the absorption band. The use of red and near-infrared wavelengths thus corresponds to measuring the abundance of one of the most vital plant pigments, chlorophyll.

Can such an interpretation be extended to narrowband indices? From the point-of-view of the physics of radiative transfer, there is no fundamental difference between broad- and narrowband indices. However, for calculating a spectral derivative, there is little use of well-tuned and potentially much noisier narrow spectral bands. For detecting pigments whose absorption spectra span tens, if not hundreds of nanometers, broadband indices seem a much more robust tool. Further, vegetation indices, especially early ones like the NDVI, have been shown both empirically and on the basis of theoretical studies, to be sensitive to factors others than those of interest, such as soil brightness changes and atmospheric effects. Most narrowband indices can be viewed as finely tuned versions of their older broadband counterparts. Site-specific selection of wavelengths leads to a better explanatory power of narrowband VIs as we also demonstrated in this case study. Unfortunately, the fine tuning for eliminating environmental effects makes narrowband indices potentially even more site-specific than broadband ones.

The comparison of narrowband and broadband VIs presented above did not concern indices capturing truly narrowband effects, e.g. the photochemical reflectance index PRI (Gamon et al., 1992) or various red edge parameters. Intrinsically narrowband VIs are based on effects that cannot be detected from broadband data. These indices are not more site-specific than broadband indices and do indeed, due to a finer spectral resolution, provide additional information on vegetation cover on all scales. Similarly, the red edge parameters calculated above make use of the high spectral resolution of narrowband data in a manner which is not site-specific. Therefore, it is not surprising that they provide a good fit for estimating forest stand variables regardless of dominating species.

An alternative to using narrowband indices would be to invert a full canopy reflectance model: the goals of both methods are to retrieve information on some biophysical variable of interest (Rautiainen et al., 2010). As discussed in this chapter, the theoretical foundations of the two approaches are somewhat similar. However, obvious limitations of index-based inversions lie in that it is not possible to define a spectral index sensitive to only one process, nor is it possible to design a universal spectral index which would be optimal for all applications everywhere and all the time (Verstraete & Pinty, 1996). Further, since vegetation indices carry only part of the information available in the

original channel reflectances, they assume that the information of interest is contained exclusively in the observed spectral variations. VIs also often neglect the effects of surface anisotropy associated with the specific geometry of illumination and observation at the time of the measurements (Govaerts et al., 1999). Last, but not least, a fundamental shortcoming of the index-based approach lies in its potentially wide application area. A user not directly working in the field of remote sensing science may be distracted by a statistically strong dependence between a variable of interest (e.g. an ecological parameter describing diversity) and a vegetation index. However, canopy reflectance signals can carry information only on what are known as state variables of radiative transfer (abundances of optically active substances, canopy amount and structure, etc.). Other variables may be correlated with one or more of the state variables, but before drawing conclusions based on such correlations, the nature and application range of the correlation should be clarified.

Naturally, physical canopy reflectance models are immune to the problems listed above. When working in the forward mode, a modern reflectance model can reliably predict the spectral reflectance signal of a vegetation canopy given the required inputs (e.g. Widlowski et al., 2007). When run in inverse mode, the models should be able to produce an estimate of the state variables of radiative transfer based on measured spectral reflectance values. Unfortunately, due to the large number of the state variables and the mathematical nature of the inverse problem, a robust result is difficult to achieve (Baret & Buis, 2008). Despite the present-day problems with inverting canopy reflectance models, it is clear that physical models hold a clear advantage over index-based biophysical parameter estimation, especially when using imaging spectroscopy data. Physical models account for changes in environmental conditions and estimate all state variables simultaneously. They also have the advantage of failing if unphysical data is fed to them (e.g. due to sensor failure or preprocessing error) instead of producing unrealistic results. The problem with the large number of state variables can be solved by the larger information content of imaging spectroscopy data (compared with that produced by multispectral sensors) and development of novel physically based parameterizations allowing a more efficient description of canopy structure. However, until the full potential of imaging spectroscopy has been utilized by the developers of physical models, narrowband vegetation indices remain valuable tools in exploring the richness of high spectral resolution data.

4. Acknowledgment

We thank Anu Akujärvi for assisting in the field measurements. This study was funded by Emil Aaltonen Foundation, University of Helsinki Research and Postdoctoral Funds, and the Academy of Finland. Hyperion EO-1 data was available courtesy of the U.S. Geological Survey.

5. References

- Asner, G.P. (1998). Biophysical and biochemical sources of variability in canopy reflectance. *Remote Sensing of Environment*, Vol. 64, No. 3, (June 1998), pp. 234-253, ISSN 0034-4257

- Baret, F., Buis & S. (2008), Estimating canopy characteristics from remote sensing observations: review of methods and associated problems, In: *Advances in Land Remote Sensing: System, Modeling, Inversion and Application*, S. Liang (ed.), pp. 173-201, Springer-Verlag, ISBN 978-1-4020-6449-4, Heidelberg
- Baret, F., Guyot, G. (1991). Potentials and limits of vegetation indices for LAI and APAR assessment. *Remote Sensing of Environment*, Vol. 35, No. 2-3, (February-March 1991), pp. 161-173, ISSN 0034-4257.
- Barry, P. (2001). *EO-1/ Hyperion Science Data User's Guide, Level 1_B*, TRW Space, Defense & Information Systems, Redondo Beach, California, USA
- Birth, G. S. & McVey, G. R. (1968) Measuring the color of growing turf with a reflectance spectrometer. *Agronomy Journal*, Vol. 60 No. 6, (March 1968), pp. 640-643, ISSN: 0002-1962
- Black, T.A., Chen, J.M., Lee, X. & Sagar, R.M.. (1991). Characteristics of shortwave and longwave irradiances under a Douglas fir forest stand. *Canadian Journal of Forest Research* Vol. 21, No. 7, (July 1991), pp. 1020-1028, ISSN 0045-5067
- Blackburn, G. A. (1998). Spectral indices for estimating photosynthetic pigment concentrations: a test using senescent tree leaves. *International Journal of Remote Sensing*, Vol. 19, No. 4, (March 1998), pp. 657-675, ISSN 0143-1161
- Blackburn, G. A. (2002). Remote sensing of forest pigments using airborne imaging spectrometer and LIDAR imagery. *Remote Sensing of Environment*, Vol. 82, No. 2-3, (October 2002), pp. 311-321, ISSN 0034-4257.
- Brantley, S.T., Zinnert, J.C. & Young, D.R. (2011). Application of hyperspectral vegetation indices to detect variations in high leaf area index temperate shrub thicket canopies. *Remote Sensing of Environment* Volume 115, Issue 2, (February 2011), pp. 514-523, ISSN 0034-4257
- Broge, N.H. & Leblanc, E. (2000) Comparing prediction power and stability of broadband and hyperspectral vegetation indices for estimation of green leaf area index and canopy chlorophyll density. *Remote Sensing of Environment*, Vol. 76, No. 2, (May 2000), pp. 156-172, ISSN 0034-4257
- Brown, L., Chen, J.M., Leblanc, S.G. & Cihlar, J. (2000). A shortwave infrared modification to the simple ratio for LAI retrieval in boreal forests: An image and model analysis. *Remote Sensing Environment*, Vol. 71, No. 1, (January 2000), pp. 16-25, ISSN 0034-4257.
- Butera, M.K. (1986). A Correlation and Regression Analysis of Percent Canopy Closure Versus TMS Spectral Response for Selected Forest Sites in the San Juan National Forest, Colorado. *IEEE Transactions on Geoscience and Remote Sensing*, Vol. GE-24, No. 1, (January 1986), pp. 122-129, ISSN 0196-2892.
- Carlson, T.N. & Ripley, D.A. (1998). On the Relation between NDVI, Fractional Vegetation Cover, and Leaf Area Index. *Remote Sensing of Environment*, Vol. 62, No. 3, (December 1997), pp. 241-252, ISSN 0034-4257.
- Chen, J.M. (1996). Evaluation of vegetation indices and modified simple ratio for Boreal applications. *Canadian Journal of Remote Sensing*, Vol. 22, No. 3, (June 1996), pp. 229-242, ISSN 0703-8992.

- Chen, J.M. & Black T.A. (1991). Measuring leaf-area index of plant canopies with branch architecture. *Agricultural and Forest Meteorology* Vol. 57, No. 1-3, (December 1991), pp. 1-12, ISSN 0168-1923
- Chen, J.M. & Black, T.A. (1992). Defining leaf area index for non-flat leaves. *Plant Cell & Environment*, Vol. 15, No. 4, (May 1992), pp. 421-429, Online ISSN 1365-3040
- Chen, J. & Cihlar, J. (1996). Retrieving leaf area index of boreal conifer forests using Landsat TM images. *Remote Sensing of Environment* Vol. 55, No. 2, (February 1996), pp. 153-162, ISSN 0034-4257
- Chen, J., Pavlic, G., Brown, L., Cihlar, J., Leblanc, S., White, P., Hall, R., Peddle, D., King, D., Trofymow, J., Swift, E., Van der Sanden, J., & Pellikka, P. (2002). Derivation and validation of Canada-wide coarse-resolution leaf area index maps using high-resolution satellite imagery and ground measurements. *Remote Sensing of Environment*, Vol. 80, No. 1, (April 2002), pp. 165-184, ISSN 0034-4257.
- Curran, P.J. (1989). Remote Sensing of Foliar Chemistry. *Remote Sensing of Environment*, Vol. 30, No. 3, (December 1989), pp. 271-278, ISSN 0034-4257.
- Danson, F. M., & Plummer, S. E., 1995, Red edge response to forest leaf area index. *International Journal of Remote Sensing*, 1995, Vol. 16, No. 1, (January 1995), pp. 183-188, ISSN 0143-1161
- Dawson, T.P. & Curran, P.J. (1998). A new technique for interpolating the reflectance red edge position. *International Journal of Remote Sensing*, Vol. 19, No. 11, (July 1998), pp. 2133-2139, ISSN 0143-1161
- Deblonde, G., Penner, M. & Royer, A. (1994). Measuring Leaf Area Index with LI-COR LAI-2000 in Pine Stands. *Ecology*. Vol. 75, No. 5, (July 1994), pp. 1507-1511, ISSN 00129658
- Deng, F., Chen, J., Plummer, S., Chen, M. & Pisek, J. (2006). Algorithm for global leaf area index retrieval using satellite imagery. *IEEE Transactions on Geoscience and Remote Sensing*, Vol. 44, No. 8, (August 2006), pp. 2219-2229, ISSN 0196-2892
- Eklundh, L., Harrie, L. & Kuusk, A. (2001). Investigating relationships between Landsat ETM+ sensor data and leaf area index in a boreal conifer forest. *Remote Sensing of Environment*, Vol. 78, No. 3, (December 2001), pp. 239-251, ISSN 0034-4257
- Eriksson, H., Eklundh, L., Kuusk, A., & Nilson, T. (2006). Impact of understory vegetation on forest canopy reflectance and remotely sensed LAI estimates. *Remote Sensing of Environment*, Vol. 103, No. 4, (August 2006), pp. 408-418, ISSN 0034-4257
- Fernandes, R., Butson, C., Leblanc, S. & Latifovic, R. (2003). Landsat-5 TM and Landsat-7 ETM+ based accuracy assessment of leaf area index products for Canada derived from SPOT-4 VEGETATION data. *Canadian Journal of Remote Sensing*, Vol. 29, No. 2, (April 2003), pp. 241-258, ISSN 0703-8992.
- Fernandes, R., Leblanc, S., Butson, C., Latifovic, R. & Pavlic, G. (2002). Derivation and evaluation of coarse resolution LAI estimates over Canada. In: *Proceedings of Geosciences and Remote Sensing Symposium*, 2002. IGARSS 02.2002, IEEE International Publications, Vol. 4, pp. 2097-2099, ISBN 0-7803-7536-X
- Gamon, J., Penuelas, J., & Field, C. (1992). A narrow-waveband spectral index that tracks diurnal changes in photosynthetic efficiency. *Remote Sensing of Environment*, Vol. 41, No. 1, (July 1992), pp. 35-44, ISSN 0034-4257

- Gao, B.-C. (1996). NDWI-A normalized difference water index for remote sensing of vegetation liquid water from space. *Remote Sensing of Environment*, Vol. 58, No. 3, (December 1996), pp. 257-266, ISSN 0034-4257.
- Gitelson, A. A., Kaufmann, Y. J. & Merzlyak, M. N. (1996) Use of a green channel in remote sensing of global vegetation from EOS-MODIS. *Remote Sensing of Environment*, Vol. 58, No. 3 (December 1996), pp. 289-298, ISSN 0034-4257
- Gong, P., Pu, R., Biging, G.S. & Larrieu, M.R. (2003). Estimation of forest leaf area index using vegetation indices derived from Hyperion hyperspectral data. *IEEE Transactions on Geoscience and Remote Sensing* Vol. 41, No. 6, (June 2003), pp. 1355-1362, ISSN 0196-2892
- Goodenough, D.G., Dyk, A., Niemann, K.O., Pearlman, J.S., Chen, H., Han, T. Murdoch, M. & West, C. (2003). Processing Hyperion and ALI for Forest Classification. *IEEE Transactions on Geoscience and Remote Sensing*, Vol. 41, No. 6, (June 2003), pp. 1321-1331, ISSN 0196-2892
- Govaerts, Y. M., Verstraete, M. M., Pinty, B. & Gobron, N. (1999). Designing optimal spectral indices: a feasibility and proof of concept study. *International Journal of Remote Sensing*, Vol. 20, No. 9, (June 1999), pp. 1853-1873, ISSN 0143-1161
- Häme, T. (1991). Spectral interpretation of changes in forest using satellite scanner images. *Acta Forestalia Fennica*, Vol. 222, The Society of Forestry in Finland & The Finnish Forest Research Institute, ISBN 951-651-092-2, Helsinki
- Heiskanen, J., Rautiainen, M., Korhonen, L., Möttöus, M., Stenberg, P. (2011). Retrieval of boreal forest LAI using a forest reflectance model and empirical regressions. *International Journal of Applied Earth Observation and Geoinformation*, Vol. 13, No. 4, (August 2011), pp. 595-606, ISSN 0303-2434.
- Horler, D.N.H. & Ahern, F.J. (1986). Forestry information content of Thematic Mapper data. *International Journal of Remote Sensing*, Vol. 7, No. 3, (January 1986), pp. 405-428, ISSN 0143-1161.
- Huete, A.R. (1988) A soil-adjusted vegetation index (SAVI). *Remote Sensing of Environment*, Volume 25, Issue 3, (August 1988) , Pages 295-309, ISSN 0034-4257
- Huete, A., Didan, K., Miura, T., Rodrigues, E.P., Gao, X. & Ferreira, L.G. (2002). Overview of the radiometric and biophysical performance of the MODIS vegetation indices. *Remote Sensing of Environment*, Vol. 83, No. 1-2, (November 2002), pp. 195-213, ISSN 0034-4257.
- Jupp, D.L.B., Datt, B., Lovell, J., Campbell, S., King, E., et al. (2002). *Discussions around Hyperion data: background notes for the Hyperion data users workshop*. CSIRO Earth Observation Centre, Canberra. (accessed: 10.10.2011), Available from ftp://ftp.eoc.csiro.au/pub/djupp/Hyperion/Workshop/Minimal_Set/Document s/Hyp_Wsn.pdf
- Jonckheere, I., Fleck, S., Nackaerts, K., Muys, B., Coppin, P., Weiss, M. & Baret, F. (2004). Reviews of methods for in situ leaf area index determination. Part I. Theories, sensors, and hemispherical photography. *Agricultural and Forest Meteorology*, Vol. 121, No. 1-2, (January 2004), pp. 19-35, ISSN 0168-1923
- Kokaly, R. F., Asner, G.P., Ollinger, S.V., Martin, M.E. & Wessman, C.A. (2009). Characterizing canopy biochemistry from imaging spectroscopy and its application

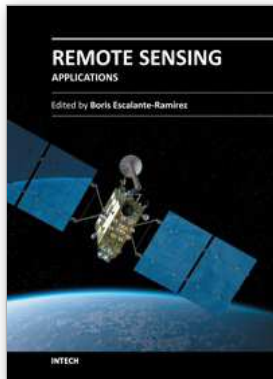
- to ecosystem studies. *Remote Sensing of Environment*, Vol. 113, Supplement 1, (September 2009), pp. S78-S91, ISSN 0034-4257
- Lang, A.R.G. (1986). Leaf area and average leaf angle from transmission of direct sunlight. *Australian Journal of Botany*, Vol. 34, No. 3, (May 1986), pp. 349 - 355. ISSN 0067-1924
- Lee, K.-S., Cohen, W. B., Kennedy, R. E., Maiersperger, T. K. & Gower, S. T. (2004) Hyperspectral versus multispectral data for estimating leaf area index in four different biomes. *Remote Sensing of Environment*, Vol. 91, No. 3-4, (June 2004), pp. 508-520, ISSN 0034-4257.
- LI-COR (1992). *LAI-2000 Plant Canopy Analyzer: Instruction Manual*. Lincoln, Nebraska, LI-COR, Inc.
- le Maire, G., François, C., Soudani, K., Berveiller, D., Pontailier, D., Bréda, N., Genet, H., Davi, H. & Dufrêne, E. (2008). Calibration and validation of hyperspectral indices for the estimation of broadleaved forest leaf chlorophyll content, leaf mass per area, leaf area index and leaf canopy biomass. *Remote Sensing of Environment*, Vol. 112, No. 10, (October 2008), pp. 3846-3864, ISSN 0034-4257
- Matthew, M. W., Adler-Golden, S. M., Berk, A., Richtsmeier, S. C., Levine, R. Y., Bernstein, L. S., Acharya, P. K., Anderson, G. P., Felde, G. W., Hoke M. P., Ratkowski, A., Burke, H.-H., Kaiser, R. D., & Miller, D. P., (April 2000). Status of Atmospheric Correction Using a MODTRAN4-based Algorithm. In: *SPIE Proceedings, Algorithms for Multispectral, Hyperspectral, and Ultraspectral Imagery VI*. Vol. 4049, Accessed (10.10.2011), Available from: <http://www.dtic.mil/cgi-bin/GetTRDoc?AD=ADA447767&Location=U2&doc=GetTRDoc.pdf>
- Miller, J.B. (1967). A formula for average foliage density. *Australian Journal of Botany*, Vol. 15, No. 1, (February 1967), pp. 141 - 144, ISSN 0067-1924
- Monsi, M. & Saeki, T. (1953). Über den Lichtfactor in den Pflanzengesellschaften und seine bedeutung für die Stoff-production. *Japanese Journal of Botany*, Vol. 14, (March 1953) pp. 22-52, ISSN 0075-3424
- Monteith, J.L. & Moss, C.J. (1977). Climate and the efficiency of crop production in Britain. *Philosophical Transactions of the Royal Society B*. Vol. 281, No. 980, (November 1977), pp. 277-294. Online ISSN 1471-2970
- Morisette, J.T., Baret, F., Privette, J. L., Myneni, R.B., Nickeson, J., Garrigues, S., Shabanov, N., Weiss, M., Fernandes, R., Leblanc, S., Kalacska, M., Sánchez-Azofeifa, G. A., Chubey, M., Rivard, B., Stenberg, P., Rautiainen, M., Voipio, P., Manninen, T., Pilant, A., Lewis, T., Iames, J., Colombo, R., Meroni, M., Busetto, L., Cohen, W., Turner, D., Warner, E.D., Petersen, G.W., Seufert, G. & Cook, R. (2006). Validation of global moderate resolution LAI Products: a framework proposed within the CEOS Land Product Validation subgroup. *IEEE Transaction on Geosciences and Remote Sensing*, Vol. 44, No. 7, (July 2006), pp. 1804-1817, ISSN 0196-2892
- Mutanga, O. & Skidmore, A.K. (2004). Narrow band vegetation indices overcome the saturation problem in biomass estimation. *International Journal of Remote Sensing*, Vol. 25, No. 19, (October 2004), pp. 3999-4014, ISSN 0143-1161
- Myneni, R. B., Hall, F. G., Sellers, P. J. & Marshak, A. L. (1995) Interpretation of spectral vegetation indexes. *IEEE Transactions on Geoscience and Remote Sensing*. Vol. 33, No. 2, (March 1995), pp. 481-486, ISSN 0196-2892

- Myneni, R.B., Nemani, R.R. & Running, S.W. (1997). Estimation of global leaf area index and absorbed PAR using radiative transfer models. *IEEE Transactions on Geoscience and Remote Sensing*, Vol. 35, No. 6, (November 1997), pp. 1380-1393, ISSN 0196-2892.
- Nemani, R., Pierce, L., Running, S. & Band, L. (1993). Forest ecosystem processes at the watershed scale: sensitivity to remotely-sensed Leaf Area Index estimates. *International Journal of Remote Sensing*, Vol. 14, No. 13, pp. 2519-2534, ISSN 0143-1161
- Nilson, T. (1971). A theoretical analysis of the frequency of gaps in plant stands. *Agricultural Meteorology*, Vol. 8, pp. 25-38, ISSN 0002-1571
- Nilson, T. & Peterson, U. (1994). Age dependence of forest reflectance: analysis of main driving factors. *Remote Sensing of Environment*, Vol. 48, No. 3, (June 1994), pp. 319-331, ISSN 0034-4257.
- Norman, J. & Jarvis, P. (1975). Photosynthesis in Sitka spruce (*Picea sitchensis* (Bong.) Carr.). V. Radiation penetration theory and a test case. *Journal of Applied Ecology*, Vol. 12, No. 3, (December 1975), pp. 839-877, ISSN 00218901
- Pearlman, J. S., Barry, P.S., Segal, C. C., Shepanski, J., Beiso, D. & Carman, S. L. (2003) Hyperion, a space-based imaging spectrometer. *IEEE Transactions on Geoscience and Remote Sensing*, Vol. 41, No. 6, (June 2003), pp. 1160-1173, ISSN 0196-2892
- Pisek, J., Rautiainen, M., Heiskanen, J. & Möttöus, M. (2012). Retrieval of seasonal dynamics of forest understory reflectance in a Northern European boreal forest from MODIS BRDF data. *Remote Sensing of Environment*, Vol. 17, pp. 464-468, ISSN 0034-4257
- Pu, R., Gong, P., Biging, G.S. & Larrieu, M.R. (2003). Extraction of Red Edge Optical Parameters From Hyperion Data for Estimation of Forest Leaf Area Index. *IEEE Transaction on Geosciences and Remote Sensing* Vol. 41, No. 4, (April 2003), pp. 916-921, ISSN 0196-2892
- Pu, R., Gong, P. & Yu, Q. (2008) Comparative analysis of EO-1 ALI and Hyperion, and Landsat ETM+ data for mapping forest crown closure and leaf area index. *Sensors* 2008, Vol. 8, No. 6, (June 2008), pp. 3744-3766, ISSN 1424-8220
- Rautiainen, M., Heiskanen, J., Eklundh, L., Möttöus, M., Lukeš, P. & Stenberg, P. (2010), Ecological applications of physically based remote sensing methods. *Scandinavian Journal of Forest Research* Vol. 25, No. 4, (July 2010), pp. 325–339, ISSN 0282-7581
- Rautiainen, M. & Stenberg, P. (2005). Application of photon recollision probability in simulating coniferous canopy reflectance. *Remote Sensing of Environment*, Vol. 96, No. 1, (May 2005), pp. 98-107, ISSN 0034-4257
- Rautiainen, M.; Möttöus, M.; Heiskanen, J.; Akujärvi, A.; Majasalmi, T. & Stenberg, P. (2011). Seasonal reflectance dynamics of common understory types in a northern European boreal forest. *Remote Sensing of Environment*, in press, (available online since 27 July 2011), ISSN 0034-4257
- Rautiainen, M., Suomalainen, J., Möttöus, M., Stenberg, P., Voipio, P., Peltoniemi, J. & Manninen, T. (2007). Coupling forest canopy and understory reflectance in the Arctic latitudes of Finland. *Remote Sensing of Environment*, Vol. 110, No. 3, (October 2007), pp. 332-343, ISSN 0034-4257
- Roberts, D., Ustin, S., Ogunjemiyo, S., Greenberg, J., Dobrowski, S., Chen, J. & Hinckley, T. (2004). Spectral and structural measures of northwest forest vegetation at leaf to landscape scales. *Ecosystems*, Vol. 7, No. 5, (May 2004), pp. 545-562. ISSN 1432-9840

- Rock, B. N., Vogelmann, J. E., Williams, D. L., Vogelmann, A. F. & Hoshizaki, T. (1986). Remote Detection of Forest Damage. *Bio Science*, Vol. 36, No. 7, (July-August 1986), pp. 439-445, ISSN 0006-3568
- Rouse, J. W., Haas, R. H., Schell, J. A. & Deering, D. W. (1974). Monitoring Vegetation Systems in the Great Plains with ERTS. In: *Third ERTS Symposium*, pp. 309-317, NASA SP-351 I, United States
- Samiappan, S., Prasad, S., Bruce, L.M. & Robles, W. (2010) NASA's upcoming HypSPIRI Mission - Precision vegetation mapping with limited ground truth. *Geoscience and Remote Sensing Symposium (IGARSS), 2010 IEEE International*, (July 2010), pp. 3744-3747. ISSN 2153-6996
- San, B. T., & M. L. Suzen, (2010), Evaluation of Different Atmospheric Correction Algorithms for EO-1 Hyperion Imagery, *International Archives of the Photogrammetry, Remote Sensing and Spatial Information Science*, Volume XXXVIII, Part 8, (August 2010), pp. 392-397, ISSN 1682-1777
- Schlerf, M. et al. (2005). Remote sensing of forest biophysical variables using HyMap imaging spectrometer data. *Remote Sensing of Environment*, Vol. 95, No. 2, (March 2005), pp. 177-194, ISSN 0034-4257
- Schull, M., Knyazikhin, Y., Xu, L., Samanta, A., Carmona, P., Lepine, L., Jenkins, J., Ganguly, S. & Myneni, R. (2011). Canopy spectral invariants, Part 2: Application to classification of forest types from hyperspectral data. *Journal of Quantitative Spectroscopy and Radiative Transfer*, Vol.112, No.4, (March 2011), pp. 736-750, ISSN 0022-4073
- Segl, K., Guanter, L., Kaufmann, H., Schubert, J., Kaiser, S., Sang, B. & Hofer, S. (2010) Simulation of spatial sensor characteristics in the context of the EnMAP hyperspectral mission. *IEEE Transactions on Geoscience and Remote Sensing*, Vol.48, No. 7, (July 2010), pp. 3046-3054, ISSN 0196-2892
- Sellers, P.J. (1985). Canopy reflectance, photosynthesis and transpiration. *International Journal of Remote Sensing*, Vol. 6, No. 8, pp. 1335-1372, ISSN 0143-1161
- Shinozaki, K., Yoda, K, Hozumi, K. & Kira, T. (1964). A quantitative analysis of plant form - the pipe model theory. I. Basic analyses. *Japanese Journal of Ecology*, Vol. 14, No. 3, (June 1964), pp. 97-105, ISSN 0021-5007
- Sims, D.A. & Gamon, J.A. (2002). Relationships between leaf pigment content and spectral reflectance across a wide range of species, leaf structures and developmental stages. *Remote Sensing of Environment*, Vol. 81, No. 2-3, (August 2002), pp. 337-354, ISSN 0034-4257
- Smith, N.J., Chen, J.M. & Black, T.A. (1993). Effects of clumping on estimates of stand leaf area index using the LI-COR LAI-2000. *Canadian Journal of Forest Research*, Vol. 23, No. 9, pp. 1940-1943, ISSN 0045-5067
- Spanner, M.A., Pierce, L.L., Peterson, D.L. & Running, S.W. (1990). Remote sensing of temperate coniferous forest leaf area index: the influence of canopy closure, understory vegetation and background reflectance. *International Journal of Remote Sensing*. Vol. 11, No.1, pp. 95-111, ISSN 0143-1161
- Stenberg, P. (2006). A note on the G-function for needle leaf canopies. *Agricultural and Forest Meteorology*, Vol. 136, No. 1-2, (January 2006), pp 76-79, ISSN 0168-1923

- Stenberg, P., Linder, S., Smolander, H. & Flower-Ellis, J. (1994). Performance of the LAI-2000 plant canopy analyzer in estimating leaf area index of some Scots pine stands. *Tree Physiology*, Vol. 14, No. 7-8-9, (July 1994), pp. 981-995, Online ISSN 1758-4469
- Stenberg, P., Rautiainen, M., Manninen, T., Voipio, P. & Smolander, H. (2004). Reduced Simple Ratio better than NDVI for estimating LAI in Finnish pine and spruce stands. *Silva Fennica*, Vol. 38, No. 1, (March 2004), pp. 3-14, ISSN 0037-5330.
- Sun, L., Neville, R., Staenz, K., & White, H.P. (2008). Automatic destriping of Hyperion imagery based on spectral moment matching. *Canadian Journal for Remote Sensing*. Vol. 34, Supplement 1, (May 2008), pp. 68-81, ISSN 0703-8992
- Tucker, C. J. (1979) ETM+3 and photographic infraETM+3 linear combinations for monitoring vegetation. *Remote Sensing of Environment*, 8, 127-150, ISSN 0034-4257
- Ustin, S. L., Gitelson, A.A., Jacquemoud, S., Schaepman, M., Asner, G.P., Gamon, J.A., & Zarco-Tejada, P. (2009). Retrieval of foliar information about plant pigment systems from high resolution spectroscopy. *Remote Sensing of Environment*, Vol. 113, Supplement 1, (September 2009), pp. S67-S77, ISSN 0034-4257.
- Validation of Land European Remote Sensing Instruments (VALERI) Network. Cited: 16.8.2011. Available from: <http://www.avignon.inra.fr/valeri/>
- Verstraete, M. M. & Pinty, B. (1996) Designing optimal spectral indexes for remote sensing applications. *IEEE Transactions on Geoscience and Remote Sensing*, Vol. 34, No. 5, (September 1996), pp. 1254-1265, ISSN 0196-2892
- Waring, R.H., Schroeder, P.E. & Oren, R. (1982). Application of the pipe model theory to predict canopy leaf area. *Canadian Journal of Forest Research*. Vol. 12, No. 3. (September 1982), pp. 556-560. ISSN 0045-5067
- Wilson, J.W. (1965). Stand structure and light penetration. I. Analysis by point quadrats. *Journal of Applied Ecology*, Vol. 2, No. 2, (November 1965), pp. 383-390, ISSN: 00218901
- Watson, D. (1947). Comparative physiological studies in the growth of field crops. I. Variation in net assimilation rate and leaf area between species and varieties, and within and between years. *Annales of Botany*, Vol. 11, No. 1, (January 1947), pp. 41-76, ISSN 0305-7364
- Welles, J.M. & Cohen, S. (1996). Canopy structure measurement by gap fraction analysis using commercial instrumentation. *Journal of Experimental Botany*, Vol. 47, No. 9, (September 1996), pp. 1335-1342, ISSN 0022-0957
- Widlowski, J. L., Taberner, M., Pinty, B., Bruniquel-Pinel, V., Disney, M., Fernandes, R., Gastellu-Etchegorry, J. P., Gobron, N., Kuusk, A., Lavergne, T., Leblanc, S., Lewis, P. E., Martin, E., Mottus, M., North, P. R. J., Qin, W., Robustelli, M., Rochdi, N., Ruiloba, R., Soler, C., Thompson, R., Verhoef, W., Verstraete, M. M. & Xie, D. (2007). Third Radiation Transfer Model Intercomparison (RAMI) exercise: Documenting progress in canopy reflectance models. *Journal of Geophysical Research-Atmospheres* 112, D09111, (May 2007), 28 pages, ISSN 0148-0227
- Williams, D. (1991). A comparison of spectral reflectance properties at the needle, branch, and canopy level for selected conifer species. *Remote Sensing of Environment* Vol. 35, No. 2-3, (February-March 1991), pp. 79-93, ISSN 0034-4257

- Wu, C., Han, X., Niu, Z. & Dong, J. (2010). An evaluation of EO-1 hyperspectral Hyperion data for chlorophyll content and leaf area index estimation. *International Journal of Remote Sensing*, Vol. 31, No. 4, (February 2010), pp. 1079-1086, ISSN 0143-1161
- Zarco-Tejada, P.J., Rueda, C.A. & Ustin, S.L. (2003). Water content estimation in vegetation with MODIS reflectance data and model inversion methods. *Remote Sensing of Environment*, Vol. 85, No. 1, (April 2003), pp. 109-124, ISSN 0034-4257.



Remote Sensing - Applications

Edited by Dr. Boris Escalante

ISBN 978-953-51-0651-7

Hard cover, 516 pages

Publisher InTech

Published online 13, June, 2012

Published in print edition June, 2012

Nowadays it is hard to find areas of human activity and development that have not profited from or contributed to remote sensing. Natural, physical and social activities find in remote sensing a common ground for interaction and development. This book intends to show the reader how remote sensing impacts other areas of science, technology, and human activity, by displaying a selected number of high quality contributions dealing with different remote sensing applications.

How to reference

In order to correctly reference this scholarly work, feel free to copy and paste the following:

Ellen Eigemeier, Janne Heiskanen, Miina Rautiainen, Matti Möttöus, Veli-Heikki Vesanto, Titta Majasalmi and Pauline Stenberg (2012). Narrowband Vegetation Indices for Estimating Boreal Forest Leaf Area Index, Remote Sensing - Applications, Dr. Boris Escalante (Ed.), ISBN: 978-953-51-0651-7, InTech, Available from: <http://www.intechopen.com/books/remote-sensing-applications/narrowband-vegetation-indices-for-estimating-boreal-forest-leaf-area-index>

INTECH

open science | open minds

InTech Europe

University Campus STeP Ri
Slavka Krautzeka 83/A
51000 Rijeka, Croatia
Phone: +385 (51) 770 447
Fax: +385 (51) 686 166
www.intechopen.com

InTech China

Unit 405, Office Block, Hotel Equatorial Shanghai
No.65, Yan An Road (West), Shanghai, 200040, China
中国上海市延安西路65号上海国际贵都大饭店办公楼405单元
Phone: +86-21-62489820
Fax: +86-21-62489821

© 2012 The Author(s). Licensee IntechOpen. This is an open access article distributed under the terms of the [Creative Commons Attribution 3.0 License](#), which permits unrestricted use, distribution, and reproduction in any medium, provided the original work is properly cited.